Composites: Part A 173 (2023) 107675

Contents lists available at ScienceDirect

Composites Part A

journal homepage: www.elsevier.com/locate/compositesa

Modeling formation and evolution of voids in unsaturated dual scale preforms in Resin Transfer Molding processes

Silvio Facciotto [a,*], Pavel Simacek [b], Suresh G. Advani [b], Anthony Pickett [a], Peter Middendorf [a]

[a] Institute of Aircraft Design, University of Stuttgart, Stuttgart, 70569, Germany
[b] Department of Mechanical Engineering and Center for Composite Materials, University of Delaware, Newark, 19711, DE, USA

ARTICLE INFO

Keywords:
Resin transfer moulding (RTM)
Fiber tow infiltration
Process Simulation
Finite element analysis (FEA)

ABSTRACT

Resin transfer molding (RTM) is a composite processing technique in which a fiber preform (usually consisting of fiber tows woven or stitched together) is enclosed in a cavity between two or more rigid molds before injecting resin under pressure to fill all empty spaces between the fibers. In this process preforms exhibit dual scale behavior as the pores between the fibers in a fiber tow are much smaller than the spaces between tows, hence the resin impregnates the inter- and intra-tow pores at different rates. In this research this dual scale behavior and void evolution is modeled through a multi scale approach to predict void location and distribution in a manufactured composite. For the simulation work dual scale behavior of the preform is represented by introducing one dimensional slave elements representing the network of fiber tows. This was conducted for a total of five different layups divided between two types of glass fiber preforms. The pressure calculated in the macroscopic model, and the dual scale results are then used as input in a mesoscopic model, in which the domain consists of fiber tows and gaps between them. Capillary effects are taken into account by locally modifying the values of the permeability. The use of a transparent mold with cameras allowed a comparison of dual scale flow and saturation of the tows at the mesoscopic level domain.

1. Introduction

The use of composite materials for structural applications is gaining momentum in many industries with most notable applications in aerospace, sports articles and wind turbine blades. Effective manufacturing comes with several challenges, especially when high quality and yield are paramount to mitigate production costs. Due to its simplicity in execution and ability to produce high volumes, the Resin Transfer Molding (RTM) process is being widely used in production chains. In RTM processes a dry reinforcement is closed inside a tool and filled with a liquid resin. The resin is injected through one or more inlets to impregnate the pores of the reinforcement. Once the resin arrives at the vent, the injection is discontinued and after resin cure the part is demolded. RTM is largely used in industry to produce components that have complex shapes and are relatively large. Typical parts are up to several meters in size and 2 to 5 mm thick based on their design and structural requirements. The engineering textiles used for this type of production often consist of fibers bunched together in tows and then interlaced to form the preform. Hence filling of such architectures often leads to the so-called "dual scale" flow. Dual scale flow refers to the infiltration behavior in which a liquid resin fills the space between individual fibers of a tow at a different rate than the gaps between the tows. The filling sequence of dual scale flow will vary depending on many factors such as the processing conditions, capillary effects, type and architecture of the reinforcement, orientation of the stack of layers and effects arising from the interaction between the preform and the mold (locally compacted areas, racetracking, bridging around corners etc.). Thus, the resin impregnation process and defects arising from it during filling of dry preforms is important and has been extensively studied in the last two decades. These filling mechanisms are key for understanding this infusion process and reducing or eliminating manufacturing voids caused by air entrapment. The dual scale flow phenomenon is directly linked to formation of voids during impregnation of the dry reinforcement. The tows of a reinforcement generally fill at a slower rate compared to gaps between them, entrapping air in the form of voids, which might compact, move, and get trapped at certain locations of the preform. Voids are undesirable as they reduce mechanical performance of the final manufactured component and can have detrimental effects on fatigue performance. Many authors correlate not only the degradation of mechanical properties with the content of voids [1–4], but also suggest the importance of void parameters such shape, dimensions, location and distribution [1,5–7]. High volume production parts will benefit from simulation techniques

* Corresponding author.
E-mail address: facciotto@ifb.uni-stuttgart.de (S. Facciotto).

https://doi.org/10.1016/j.compositesa.2023.107675
Received 10 March 2023; Received in revised form 9 June 2023; Accepted 30 June 2023
Available online 4 July 2023

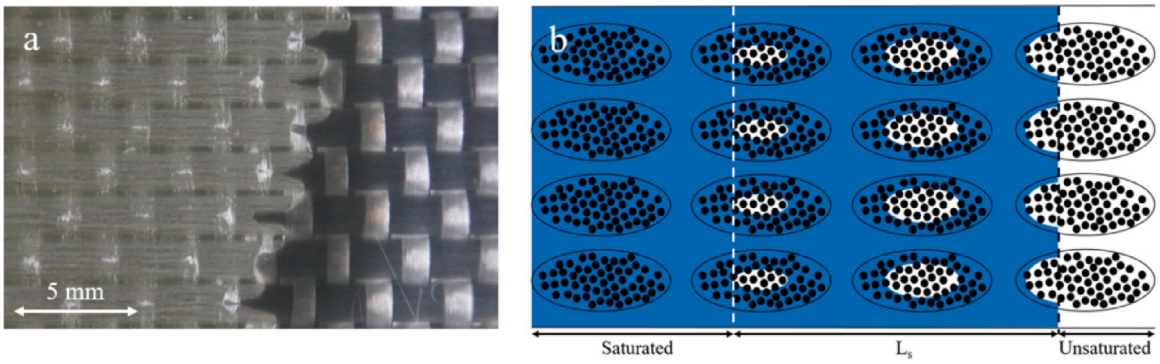

Fig. 1. Dual scale flow (Left: Experiment, Right: Schematic) [13].

capable of predicting and optimizing the outcome of the filling process to eliminate voids, thus reducing development time and production waste.

1.1. Capillary effects and dual scale flow

In RTM infiltration is normally driven by the pressure difference generated between the inlet (either applied pressure or flow rate) and the pressure conditions inside the cavity. However, capillary forces are present between fiber filaments of the tows which may also play a role in filling of the fiber tows and regions around it. Dual scale flow is directly linked to capillary forces that provide the wicking during impregnation of the dry reinforcement and thus to the capillary number. In the regions of low resin pressure gradient, the importance of capillary forces will be promoted. This was shown, amongst others, by Ruiz et al. [8] and Leclerc et al. [9] through a series of experiments to demonstrate an optimum flow front speed in order to achieve the minimum content of voids.

In general, reinforcements used in the industry present a strongly anisotropic pore structure, with highly compacted tows. The permeability values of such tows are several orders of magnitude lower compared to the permeability of bulk preforms [7,10–12]. This results in filling of tows at a much slower rate as compared to impregnating the gaps between them. Dual scale flow occurs in both unsaturated and saturated fibrous media. For the case of unsaturated preform the dual scale region is the partially filled fiber tows. This can be defined by the saturation length L_s, which is the distance between the flow front and fully saturated boundary of the preform in which tows and the region within tows are fully filled [13]. This parameter is shown in Fig. 1(b) and depends on several factors including flow velocity, type and compaction of reinforcement, flow direction and applied processing conditions. Patel and Lee performed several porosity measurements for different liquids and flow velocities [14] showing that capillary action at lower capillary numbers can generate and entrap meso scale voids up to 15% of the volume. Other authors have also shown how slow filling can lead to meso scale void formation [8,9,15,16]. Moreover, Lundström et al. numerically investigated void creation and dynamics in non-crimp fabrics showing that tiny gaps between tows, crossings and threads are common locations for generation of intra-bundle voids. Further, the authors demonstrated how the use of vacuum can effectively reduce the void fraction entrapped [17]. These studies suggest that there will be situations when the importance of capillary forces cannot be ignored while studying mold filling and saturation of preforms during manufacturing of composites.

Capillary forces within the mold between the empty spaces act in the form of pressure difference between the liquid and environmental pressure. These forces are generated by the surface tension of the injected resin with air inside the cavity, and the interfacial tension between the fibers and the resin [18]. If for example a capillary tube is considered, this pressure difference can be calculated as:

$$\Delta P_{cap} = -\frac{2\gamma cos\theta_{rc}}{r} \tag{1}$$

where γ is the surface tension between fluid and the environment, θ_{rc} is the static contact angle formed by the meniscus of liquid in the capillary tube and r is the tube radius. In Eq. (1) if $\Delta P_{cap}<0$ the system is a wetting system, whereas $\Delta P_{cap}>0$ indicates a non-wetting system [18,19]. Similar to a capillary tube, capillary action plays a role in the infiltration process between fibers of a tow in a dry preform. Engineering textiles or preforms often contain anisotropic and dual scale porous structures, where the size of pores within a bundle of fibers is several orders of magnitude smaller than the gaps between tows. Ahn et al. [20] and Pillai and Advani [21] proposed an analytical expression to calculate capillary pressure for a fiber tow:

$$\Delta P_{cap} = \frac{F}{D_f}\frac{V_f}{1-V_f}\gamma cos\theta_{rf} \tag{2}$$

where V_f is the fiber volume fraction of the tow, D_f is the diameter of a fiber inside the tow, F is a shape factor describing anisotropy of the tow and θ_{rf}, similar to Eq. (1), is the static contact angle between resin and fibers. This model has largely been used in the literature [13,22–25] along with a model proposed by Bayramli and Powell [26–29] to study the role of capillary pressure and included in the modeling. Inside a preform, capillary action is combined with viscous drag during the filling process. As reviewed by Teixidó et al. [18] capillary pressure values found in composites processes are in the range of 1000–70000 Pa. The combination of bulk permeability, a much lower tow permeability [10–12], and capillary effects contribute to the complex filling of a preform. Capillary forces are present at the interface between fluid and fiber and are strongly influenced by the velocity of the moving flow. In the literature the capillary number is used by many authors to relate fluid velocity to percentage of voids [8,9,30–33]:

$$Ca^* = \frac{Q}{A}\frac{\eta_r}{\gamma cos\theta_{rc}} \tag{3}$$

where Q is the fluid flow rate filling the pores, A is the cross section of the porous medium and η_r is the viscosity of the liquid resin. In case of viscous resins, Eq. (3) can be simplified as [18]:

$$Ca^* = \frac{Q}{A}\frac{\eta_r}{\gamma} \tag{4}$$

1.2. Modeling of voids

Dual scale flow is considered to be key to understanding and modeling formation and evolution of voids during filling of Liquid Composite Molding processes such as RTM and VARTM [1,15,34]. The saturation of tows and gaps between them has been modeled in the literature using several techniques. As reviewed by Teixidó et al. [18] a common approach to model this phenomenon is to include a sink term in the

Table 1
Reinforcement layups and reference name used in this paper.

Type of Material	Interglas 92146 (quasi-UD)	Interglas 92140 (woven)
Layup 1	$[0]_6$ - QUD 0	$[0]_7$ - WOV 0
Layup 2	$[90]_6$ - QUD 90	$[0/+45/-45/0/-45/+45/0]$ - WOV 0/45
Layup 3	$[0/90/0]_s$ - QUD 0/90	–

model [15,33–43]. In particular, this sink term was introduced by Pillai et al. [44] in the continuity equation to solve for dual scale flow in macroscopic flow problems. Ruiz et al. and Leclerc et al. [8,9] modeled the final void content starting from experimental observations and expressing it as a function of the capillary number. Park et al. modeled the generation, compaction and motion of voids numerically taking into consideration the microscopic structure of the tow [15,39]. DeValve et al. included capillary effects in simulating ideal plain weave architectures that included air entrapment mechanisms [45]. Gascon et al. modeled dual scale flow and formation and evolution of voids using a fractional flow model [46]. Liu et al. showed modeling of voids using a bifluid-solid contact model [47]. Arcila et al. [43] modeled mesoscopically the evolution of voids, including splitting, using the boundary elements method. Kang et al. and Aaboud et al. [48,49] evaluated the time necessary to fill macro and micro pores to compute generation and evolution of voids, taking into account heterogeneous permeability of fiber tows [50]. Along with these strategies, a sink term can be used adding a series of slave one-dimensional elements to the base mesh representing the bulk preform in order to analyze the dual scale behavior of the textile. This approach was proposed by Simacek and Advani [35] using the Finite Elements software Liquid Injection Molding Simulations (LIMS), that was then used in several other works [13,37,51]. Darcy's law and continuity equation are combined, including the sink term q, which is a function of saturation s and pressure P:

$$\nabla \cdot \left(\frac{\overline{\mathbf{K}}}{\eta} \cdot \nabla P \right) = q(P, s) \tag{5}$$

where $\overline{\mathbf{K}}$ is the saturated permeability of the reinforcement and η is the viscosity of the injected resin. It is important to note that when the tow is completely filled, the sink term q disappears. The additional volume added with the one dimensional elements must be accounted for to preserve the total porous volume within the mold and the fiber tow permeability must be correlated as shown by Simacek et al. [35] and in our previous work [13].

This method can be used to analyze dual scale behavior during filling, however the prediction of void content is still not included explicitly in this model. Another important consideration concerning the model in its original form [35] is that using only one slave element to model filling of tows does not account for connections between tows under consideration. This was addressed by introducing a second family of elements to enable possible movement of resin or voids along the fiber tows [13]. Yeager et al. [28] showed how LIMS can be used to analyze the void formation and evolution modeling a tow, including capillary effects that are incorporated by changing the local permeability. The method proposed in this paper consists of analyzing the dual scale process using the macroscopic "slave" elements model presented in [13] that is adapted to include different reinforcement orientations, and integrate the information gathered to predict the evolution of voids at the mesoscopic level. This is done by extracting nodal pressure values from the macroscopic model and applying it to a mesoscopic model representative of the reinforcement structure, in which the capillary pressure is modeled augmenting the tow's permeability [28] with voids computed by applying a non-zero pressure at the outlet.

2. Modeling dual scale with LIMS: macroscopic model

The model presented in this section is used to analyze dual scale flow during filling of rectangular preforms. This is done adding a network of elements acting as the sink term of (5). The model consists of a base 2D mesh representing the bulk preform, a set of sink elements representing the tows in the transverse direction and a set of sink elements connecting the tows. This method was presented in our previous work [13] and enables resin and void transportation between the network of tows. The architecture and orientation of the preform are taken into account by separating the porous spaces into groups of layers sharing a common fiber orientation. Capillary pressure is added using vents, as presented by Lawrence et al. [37]. The cavity analyzed for dual scale analysis corresponds to a simple rectangular plate with dimensions 280 mm × 205 mm and thickness 2 mm. The fibers used for this study are quasi-UD glass plain woven fabric from Interglas 92146 (425 g/m^2, with 550 tows per m (EC9-136 × 5t0) in warp direction and 630 tows per m (EC9-68) in weft direction) and glass 2 × 2 twill weave from Interglas 92140 (390 g/m^2, with 600 tows per m (EC9-68) in warp direction and 670 tows per m (EC9-272) in weft direction). In this paper, QUD and WOV will be used, respectively, as reference names for these two types of preform. For these two preforms, the layups presented in Table 1 with relative reference names were considered.

The resin used in this work is the epoxy resin system Hexion Epikote Resin MGS RIMR 235 with Hexion Epikote Curing-Agent MGS RIMH 237. The model is built starting from a two-dimensional shell mesh representing the bulk preform. At each node of the mesh a network of "slave" elements is attached as shown in Fig. 2. These slave elements are bar elements that represent the tows of the reinforcement and their connections. The dimensions of these elements are calculated starting from the base mesh generated. The mesh is prepared with regular, identical elements. If, for example, a 2D element with 5 mm edge is chosen, a 5 mm by 5 mm surface of real preform is analyzed (Fig. 3). The length of elements connecting tows within in the X-Y plane (L_{l-elem}) (plane parallel to filling plane, as shown in Fig. 2) is determined starting from the mesh that represents bulk permeability. For the elements originating from the bulk mesh nodes (orthogonal elements) the length of elements can be calculated as follows:

$$L_{t-elem} = \frac{h_{tow}}{2} n_l n_t \tag{6}$$

where h_{tow} is the minor axis of the tow simplified to fit an elliptic cross-section, n_l is the number of layers and n_t is the number of tows present in one single layer over the area analyzed. The model is built to represent two (or more) families of tows. This is used, for example, to analyze warp and weft fibers as presented in [13]. Mesh parameters are shown in Table 2. As shown in literature experimentally by Adams et al. [52] and numerically by Bancora et al. [53], stacking order of layers in preforms impacts filling mechanisms and dual scale. In this work this was simplified and for the case of more complicated layups, the groups of fibers were re-organized to represent fibers sharing the same orientation as shown in Fig. 2. This has been applied here to simulate the different dual scale lengths generated by the layers of the preform when oriented in different directions. The length of slave elements is calculated using (6) while grouping layers of fibers oriented in the same direction under the same family. As presented by Simacek et al. [35] the porous volume added with the sink elements must be accounted for and the reader is referred to [13] for a detailed description. This model is used to analyze dual scale behavior with capillary pressure implemented in the model by using extra vents placed on top of the network of bar elements representing fiber tows. The model takes into consideration the presence of capillary pressure until the tow corresponding to the vent is completely saturated and the

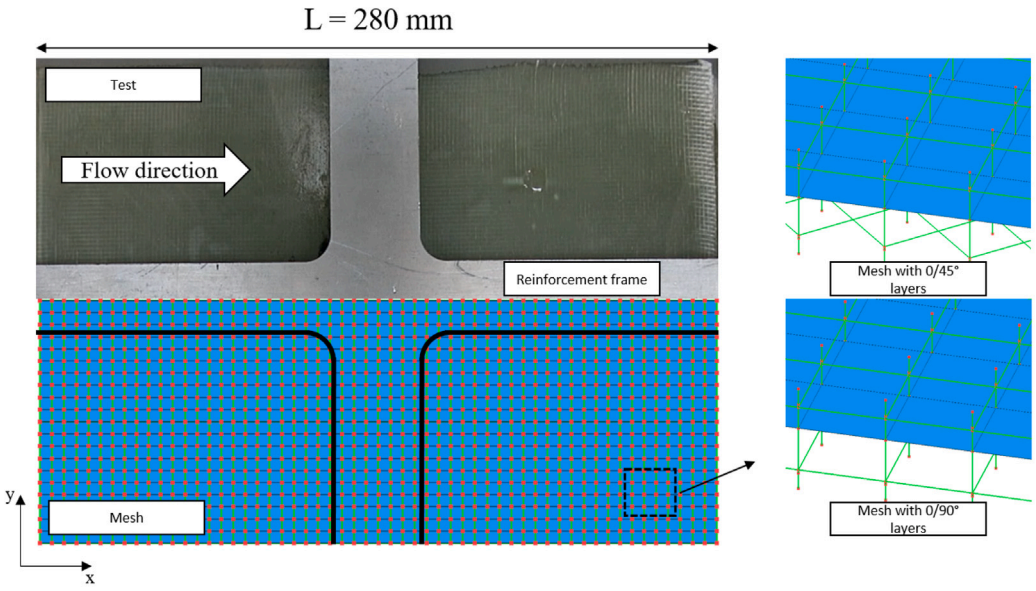

Fig. 2. Macro-model used to simulate dual scale flow.

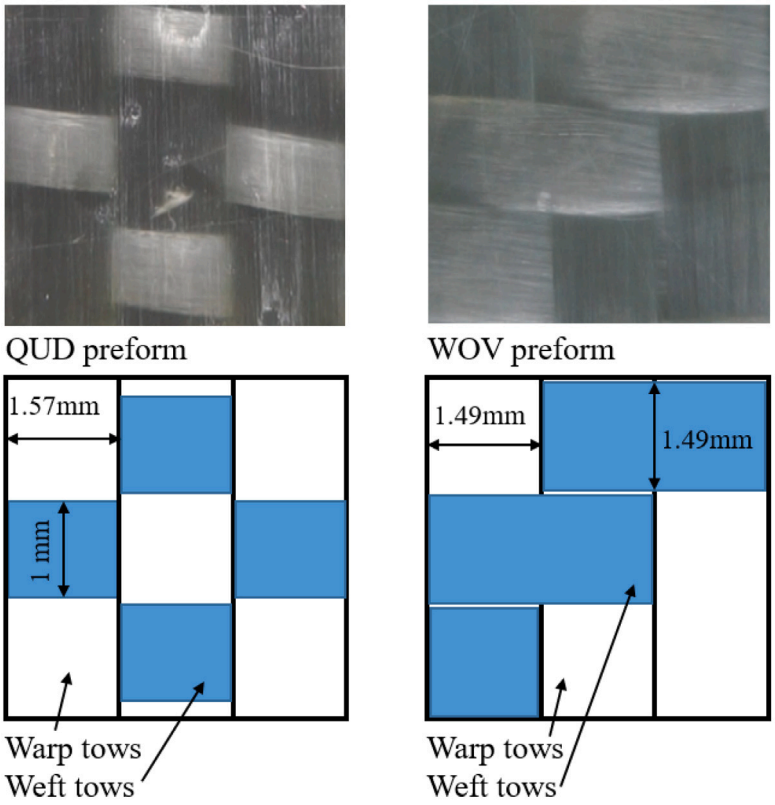

Fig. 3. Types of reinforcements, portion of preform analyzed and tow dimensions.

vent is closed. This model, originally presented by Lawrence et al. [37] was implemented in our previous work [13]. The analysis of dual scale behavior is helpful to make a first observation of possible problematic areas, assuming that an increased dual scale effect will also modify the final content of voids. This is the case, for example, when inlet and outlet conditions of the process are defined so that excessively fast or slow filling occurs. In this work, the model was used to perform a more thorough analysis by generating pressure boundary conditions for the model representing the fibers at a mesoscopic level. As shown by Kuentzer et al. and Zhou et al. the evolution of pressure is influenced by the presence of dual scale flow [51,54]. The pressure of nodes located at 75 mm from the inlet line is monitored during the filling simulation of a plate, since this corresponds to the position of the macro-lens camera used to film the filling of the fiber tows during the experiments. The information is then saved into a separate file and used as input for the mesoscopic model.

Table 2
Mesh Parameters used in Macro Model.

ID	$L_{t-elem1}$ [mm]	$L_{t-elem2}$ [mm]	$L_{l-elem1}$ [mm]	$L_{l-elem2}$ [mm]	V_{f1}	V_{f2}
QUD 0	3.3	0.675	5	5	0.69	0.63
QUD 90	0.675	3.3	5	5	0.63	0.69
QUD 0/90	2.67	1.34	5	5	0.69	0.63
WOV 0	2.2	2.2	5	5	0.701	0.701
WOV 0/45	2.5	1.9	5	$5\sqrt{2}$	0.701	0.701

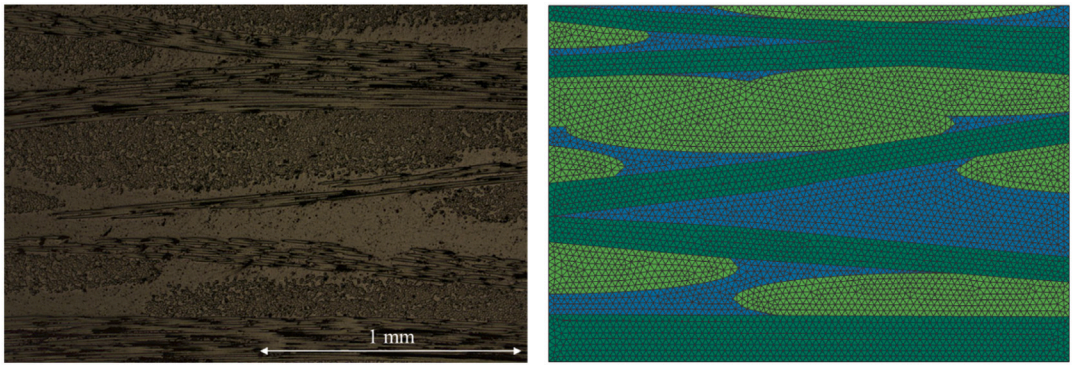

Fig. 4. Microscope section and FEM model built based on the geometry at this scale.

3. Mesoscopic model integrating dual scale flow simulation with void simulation

A mesoscopic model of the tows is prepared using microscopic sections of the two reinforcements for each layer configuration studied. This model has the scope of analyzing formation and evolution of voids and it is linked to the macroscopic simulation model. The models are built using characteristic dimensions and gaps measured from microscopic sections, however, they slightly differ from the microscopic pictures due to the assumption that tows are elliptical (Fig. 4).

Tows are considered transversely isotropic and the permeability values assigned to them are calculated using the analytical model presented by Gebart [55]:

$$K_l = \frac{8R^2}{c}\frac{(1-V_f)^3}{V_f^2} \tag{7}$$

$$K_t = C_1\left(\sqrt{\frac{V_{fmax}}{V_f}}-1\right)^{\frac{5}{2}}R^2 \tag{8}$$

where K_l and K_t are permeability in axial and transverse directions respectively, R is the radius of the fibers, V_{fmax} is the maximum volume fraction achievable and C_1 and c are constants depending on distribution of the fibers inside the tow. Values of these parameters are summarized in Table 3.

Since the mesh generated for the mesoscopic model consist of tows and gaps between them, an inter tow permeability value has to be assigned to the model. The effective permeability K_{eff} used to model these gaps is calculated using the method presented by Godbole et al. [56]:

$$K_{eff} = \frac{1}{d_{gap}+d_{tow}/2}\left(\frac{d_{gap}^3}{3}\right) - K_t\frac{L_s^2}{2(d_{gap}+d_{tow}/2)d_{tow}/2} \tag{9}$$

where d_{gap} is half of the gap thickness (inter tow region), d_{tow} is the tow minor axis, K_t is the permeability of the tow in transverse direction, and L_s is the length of the partially saturated zone (or dual scale length, Fig. 1). L_s can be obtained from experiments and macroscopic simulation results. K_{eff} was used in this study to obtain an approximate value of inter tow permeability, this was considered to be sufficient as the values of permeability calculated are for the majority of gaps in the range of $e{-}9$ m^2, about four orders of magnitude higher than tow permeability. An average gap thickness is obtained

Table 3
Parameters for permeability calculation.

Fiber arrangement	C_1	V_{fmax}	c
Quadratic	$\frac{16}{9\pi\sqrt{2}}$	$\frac{\pi}{4}$	57
Hexagonal	$\frac{16}{9\pi\sqrt{6}}$	$\frac{\pi}{2\sqrt{3}}$	53

for every gap meshed in the model and K_{eff} is kept constant within each zone and throughout the filling. The latter is again a simplification as the effective permeability model by definition is valid for unsaturated zones. This however due to the same reason mentioned above is considered acceptable for this study. The permeability of tows is adjusted to account for capillary pressure, as presented by Yeager et al. [28]. This permeability is updated at each step of the solution to account for capillary pressure for non-saturated tows. When the filling of tows is complete, the modified values are reverted to the original one calculated with Gebart's method. This model has been extended to include multiple tows, capillary pressure values (making a distinction between tows filled longitudinally and transversally), and to include the possibility to apply vacuum or atmospheric venting conditions. The pressure of voids is calculated at every iteration by LIMS and the permeability is also updated by a script to account for pressure variations during the filling process. The modified permeability value accounting for this can be expressed as:

$$K_{mod} = K_{geb}\frac{P_{cap}+P_{app}-P_{void}}{P_{app}-P_{void}} \tag{10}$$

where K_{geb} is the permeability calculated with Gebart's model [55], P_{cap} is the capillary pressure, P_{app} is the pressure applied (boundary condition) and P_{void} is the vent pressure. LIMS can account for presence of atmospheric or vacuum conditions and also analyze compression and movement of voids once the flow of resin has entrapped them. Once a void is surrounded by resin, its pressure becomes a simulated value and pressure changes inside voids are computed using the ideal gas law. Local changes in pressure result in flow rate variations, which can increase or decrease fill factor, thus resulting in void displacement but without any distinction between filling and de-filling mechanisms. This represents a simplification of voids motion and it is not intended as an accurate computation of their speed or final displacement. The model represents however a useful tool allowing an estimate of creation,

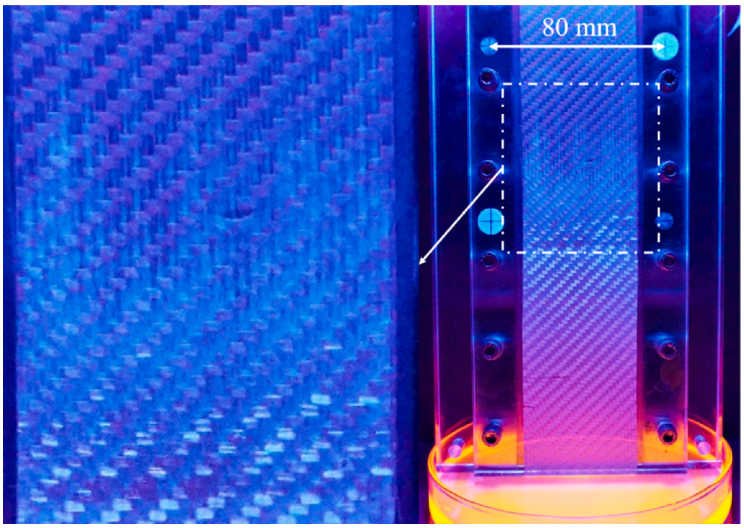

Fig. 5. Capillary wicking experiment using Rhodamine B and black light for flow visualization.

final size, pressure of voids and possible evacuation. The boundary conditions applied to the model are the pressure function obtained from the macroscopic model and atmospheric or vacuum vents, which are kept open. The inlet nodes are chosen between nodes that do not belong to the tows on one side of the mesh, while all nodes on the opposite side of the mesh are chosen as vents. The model is then executed for a selected amount of time to predict formation and evolution of voids. Alternatively, a condition can be set to obtain the time necessary to completely fill the portion of textile analyzed, keeping in mind that under atmospheric vent conditions this condition might not be met due to impossibility to evacuate the voids (for example in case of a low inlet pressure).

4. Experimental work

4.1. Capillary wicking experiments

In order to measure the effect of capillary pressure, a set of capillary wicking experiments have been run for both textiles and at different orientations and volume fractions. The testing rig consists of an adjustable cavity with dimensions 300 mm × 50 mm [57]. A single layer of preform is placed into the cavity, leaving a few mm of preform in contact with the liquid reservoir. For wicking of fibers, glycerol 86% was used. This was mixed with the colorant Rhodamine B in very small amounts (1 drop for the entire glycerol bath — corresponding to 100 ml of liquid). Rhodamine B is moreover a fluorescent colorant, which made possible testing using black-light to obtain a clear view of flow front during the entire process (Fig. 5). The measurement was performed using a digital camera with 24 megapixel definition and a standard zoom lens (16-50 mm, f/3.5–5.6) paired with a digital controller, which allowed taking pictures every 10 min. Furthermore 4 points are marked on the rig at 80 mm distance to allow measurement using image analysis. For every picture analyzed 5 different measurements are taken.

The experiment was reproduced for fibers at 0°, 90° and 45°. Moreover, the rig cavity was adjusted to achieve three different fiber volume fraction values. The method used to evaluate results of capillary wicking experiments is that proposed by Amico et al. [22] and presented by Caglar et al. [58]:

$$\frac{dh}{dt} = -\frac{K_{tow}\Delta P_{cap}}{\phi\eta}\frac{1}{h} + \frac{K_{tow}\rho g}{\phi\eta} \tag{11}$$

where h is the height reached by the liquid, t is the time, K_{tow} is the tow permeability along the dipping direction, ϕ is the porosity of the tow, η is the viscosity of the liquid, ρ is density and g is the acceleration due to gravity. Eq. (11) can be expressed in the form:

$$\frac{dh}{dt} = C_1\frac{1}{h} + C_2 \tag{12}$$

The experimental data can be fit to a first order polynomial (Fig. 6), in the form of Eq. (12) allowing the calculation of ΔP_{cap} as:

$$\Delta P_{cap} = -\rho g\frac{C_1}{C_2} \tag{13}$$

The model proposed by Amico and Lekakou [22] assumes unidirectional flow. However, in reality flow takes place inside the longitudinal tows, transverse tows and gaps between them [58,59]. Also, the tows transverse to the flow serve as liquid reservoir as shown by Mhetre et al. [60]. In this work, contrary to the testing performed by Caglar et al. [58], the single layer of preform was compacted to a desired fiber volume fraction, increasing the presence of wall effects, but also introducing compaction of the tows and thus impacting the wicking process as shown by Monaenkova et al. [61]. The results of this study can be seen in Fig. 7. Compaction influences capillary pressure, by increasing the fiber volume fraction of the material, flow will rise faster and thus capillary pressure will be stronger. It is also possible to notice a difference between reinforcements and their architecture. For the QUD preform, the capillary action is noticeably higher in one fiber orientation (0°) compared to the other. It is also higher than the WOV material. This confirms the work by Amico and Lekakou [59] and what stated in the work by Caglar et al. [58] that transverse fibers have an impact on the rise of liquid due to capillary action. Thus, the values obtained with this method might differ from values obtained with other measuring strategies, like the one presented by Pucci et al. [62] and LeBel et al. [63]. Furthermore, the accuracy of this method is limited to the pixel definition of the camera and contrast obtained between fluid and fibers during filling. Correlation coefficient R for a linear fit ranged between 0.81 for the and 0.99 showing strong correlation overall, but presenting lower values for wicking in 45° and 90° directions.

4.2. RTM experiments

The setup used for comparison of both the macroscopic and mesoscopic models consists of a two-part RTM mold (Fig. 8), where the top part is transparent acrylic glass and allows for visualization of the filling process. This is reinforced with an aluminum frame to avoid excessive bending. The geometry of filled parts corresponds to a 280 mm × 205 mm × 2 mm rectangular flat panel with resin injected into the mold cavity from a bucket that is maintained at constant pressure.

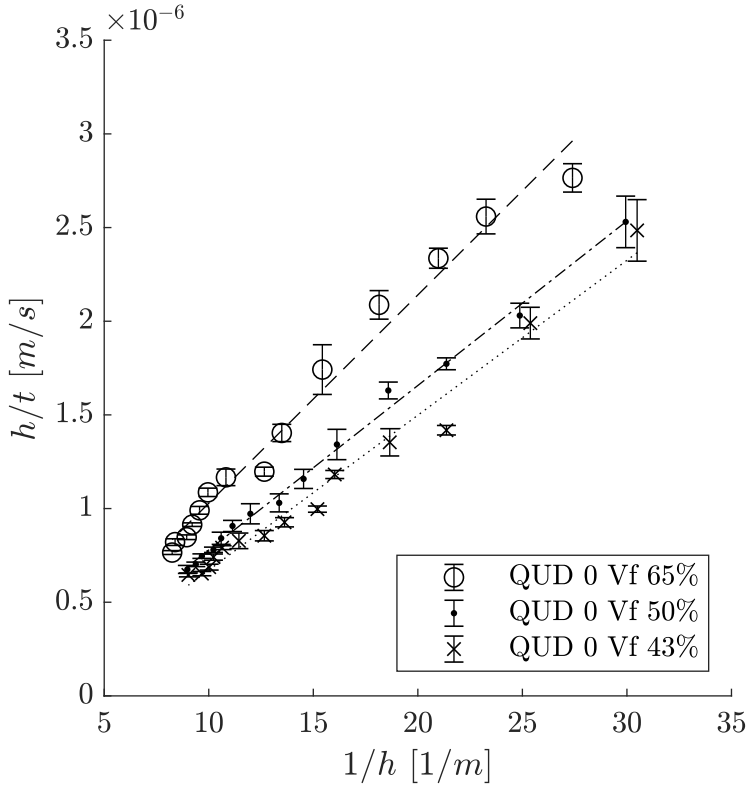

Fig. 6. QUD: polynomial fit, capillary wicking experiments in 0° direction for different compaction values.

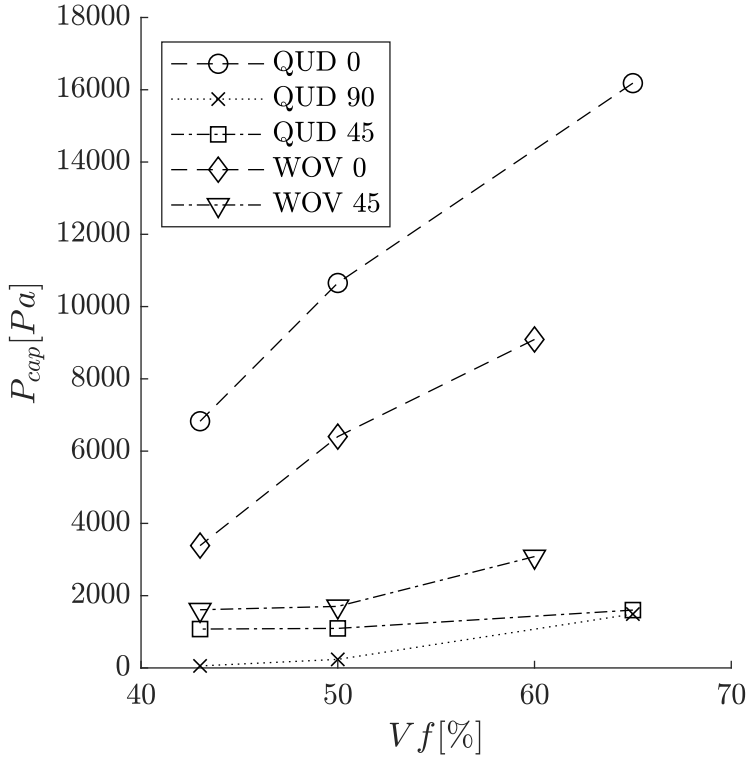

Fig. 7. Fiber volume fraction influence on capillary pressure for both fabrics and for different fiber orientations.

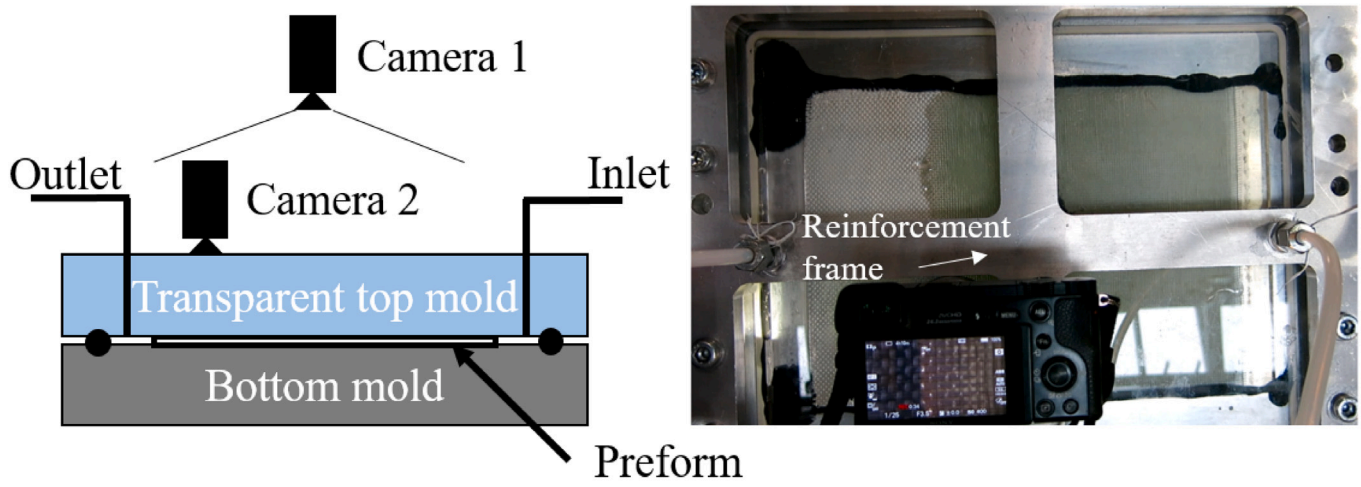

Fig. 8. RTM experimental setup. A camera films the experiment from above (camera 1), while a second camera (equipped with macro-lens) films the mesoscopic filling of tows.

Table 4
Process parameters.

ID	V_{fbulk} [%]	ΔP [Pa]	η [Pas]	K_{xxbulk} [m^2]	K_{yybulk} [m^2]
QUD 0	44	200 000	0.26	1.76E−10	1.88E−11
QUD 90	46	200 000	0.26	1.88E−11	1.76E−10
QUD 0/90	46	200 000	0.26	6.39E−11	5.25E−11
WOV 0	45	200 000	0.26	3.42E−11	1.36E−11
WOV 0/45	46	200 000	0.26	2.84E−11	1.76E−11

The filling process is recorded using a camera positioned on top of the setup, while the saturation of the tows was recorded using a second camera equipped with macro-lens and placed directly on top of the acrylic glass. The layups used in the simulation were tested for both atmospheric and vacuum outlet conditions, keeping the same constant pressure difference of 2 bars.

5. Simulation results and comparison with experimental data

5.1. Simulation of dual scale

As already shown in Section 2, the first simulation step consists of simulating dual scale using the macro-model. The simulation boundary conditions correspond to testing conditions. In this simulation step, voids are not considered, and vent pressure is assumed to be zero. The values of permeability of the bulk preform were obtained through radial permeability tests. Their values are provided in Table 4. The values of permeability of fiber tows (which are assigned to bar elements forming the network of tows), use Gebart's model [55] as a starting value. The comparison between experiments and simulation was done by optical analysis of dual scale flow through the filling (Fig. 9).

In order to visualize and measure dual scale portion of filling, a camera was mounted on top of the transparent RTM mold, to record the experiment. Optical measurements are limited, since viewing is restricted to only a portion of the preform in contact with the transparent mold top. However, the use of glass fibers does make it possible to visualize at least a few layers below the surface (Fig. 10).

This made the analysis of dual scale possible for layers of the preform with different fiber orientations. The constant inlet pressure was monitored during filling along with temperature. Experiments were performed for both atmospheric and vacuum conditions, with the aim of observing any differences in dual scale flow and filling for both cases. In some experiments, the use of a second camera with a macro lens (sony alpha 6400 with 30 mm f2.0 macro lens) was necessary to measure the length Ls of the dual scale region (Fig. 10). The images and videos obtained were converted to 8-bit images and analyzed, setting a threshold with the open source software Fiji. It should be noted that values of threshold were chosen manually. However, this was enough to obtain a first approximation of the dual scale length L_s and saturation percentage, as shown, for example, for the QUD 0/90 configuration in Fig. 11. Dual scale flow is influenced by local changes in the preform and measurements can vary depending on the area of preform analyzed. In this work the measurement of dual scale was performed taking 5 measurements of L_s along the flow front and averaging the values obtained for each time analyzed. The macro lens videos were used additionally to compare the model relative to filling of tows (meso-model) presented in the next section. Filling of the tows is clearly influenced by venting conditions, resulting in different dual scale flow behaviors of the preform as visible in Fig. 11. Results obtained from the simulation are in good agreement with tests performed under vacuum conditions. Knowing the dual scale length (Fig. 10) and flow front position (x_{ff}), the length of saturated preform x_{sat} can be calculated as $x_{sat} = x_{ff} - L_s$. Knowing the length of the plate L, the ratio x_{sat}/L can be used to describe the portion of reinforcement that has been completely saturated. In Fig. 12 this is plotted along with standard deviation against relative time t/t_{tot}, where t_{tot} is the total time necessary to fill the entire cavity. The process under vacuum conditions is characterized by a deeper saturation color and less isolated non-saturated tows behind the flow front.

Simulating atmospheric conditions was performed by adjusting the values of K/L^2_{elem} (where L_{elem} is the length of slave elements) [51] to match the dual scale behavior observed in the experiments once the resin reached the end of the preform. It can be noticed that the presence of air in the fiber tows prevents the flow of resin from saturating them completely, leaving unsaturated tows behind and increasing the dual scale length (Fig. 11). In Fig. 13 the results of simulation of dual scale of the different layups and reinforcement's type are shown, where it is clearly shown that layup and architecture, along with vent conditions strongly influence dual scale behavior of the reinforcement during filling. For the QUD preform the effect of vacuum and atmospheric filling is evident, whereas for the WOV preform this is less clear. This is noticeable in the experiments (Fig. 14) where values of L_s obtained in the experiments and their standard deviation are plot against relative time.

5.2. Simulation of void formation and filling of tows

Results obtained with the model described in Section 3 are discussed in this section. The plates infiltrated during experiments were cured and cut in small specimens, which were then analyzed with a microscope to reconstruct the geometry and simulate evolution of voids. The boundary conditions have been applied to the model to represent a linear flow

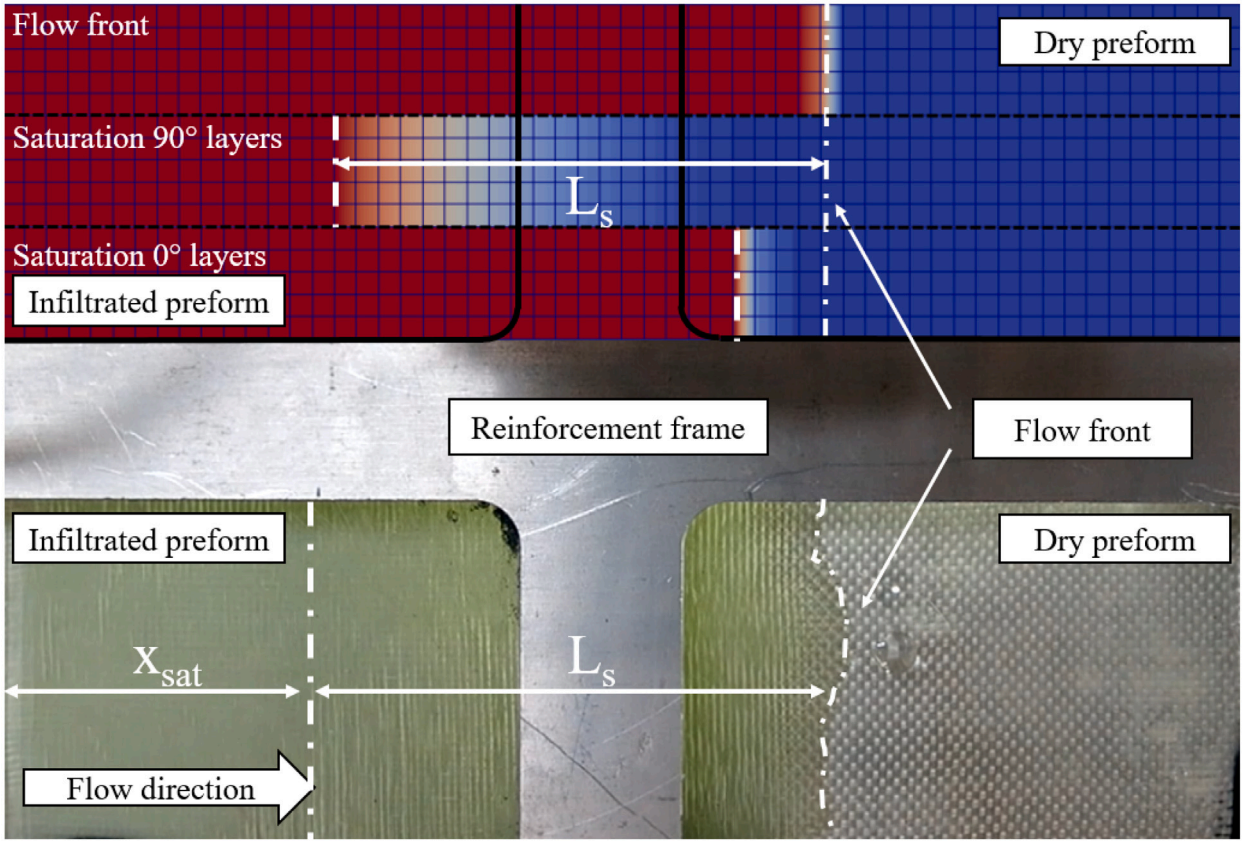

Fig. 9. Comparison between simulation and test (QUD 0/90 layup, atmospheric conditions) of the macroscopic flow front.

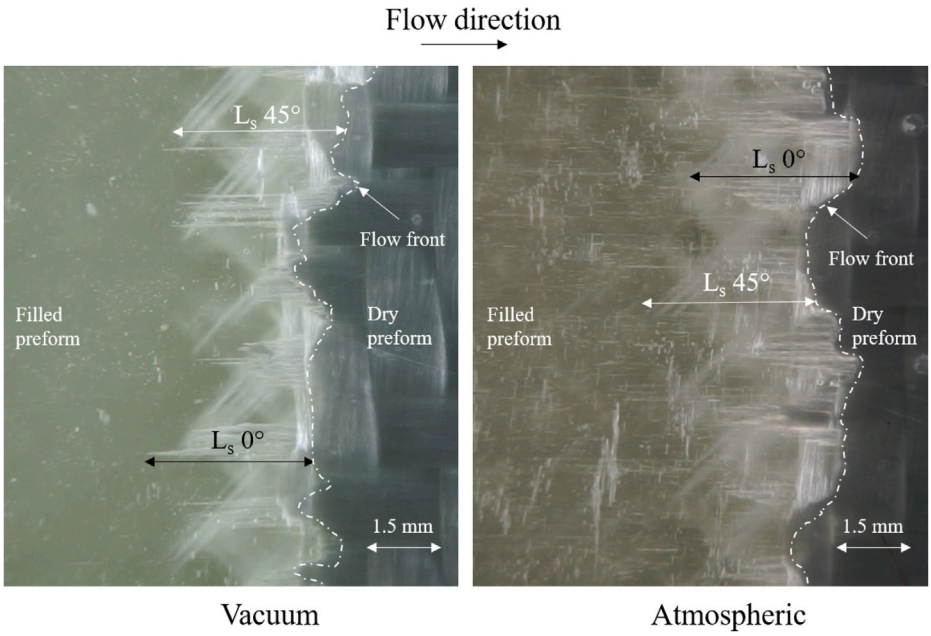

Fig. 10. Example of Dual scale length measurement (L_s) (a) WOV 0/45 vacuum and (b) atmospheric conditions for ΔP of 2 bars.

through the preform. The vents are kept open through this process to preserve flow of resin and allow compaction and movement of the voids under realistic conditions, while the inlet pressure increases with time following the pressure behavior measured in the macro model. This is obtained at the position equivalent to the macro-lens camera during the tests. The time required to saturate gaps and tows was compared to the macro-lens images obtained. This mesoscopic model can predict void entrapment and evolution under atmospheric and vacuum conditions. A sensitivity study was performed to analyze the impact of capillary pressure during the filling. This was done for the QUD 0/90 layup, applying the capillary pressure values indicated in Table 5 for both atmospheric and vacuum conditions.

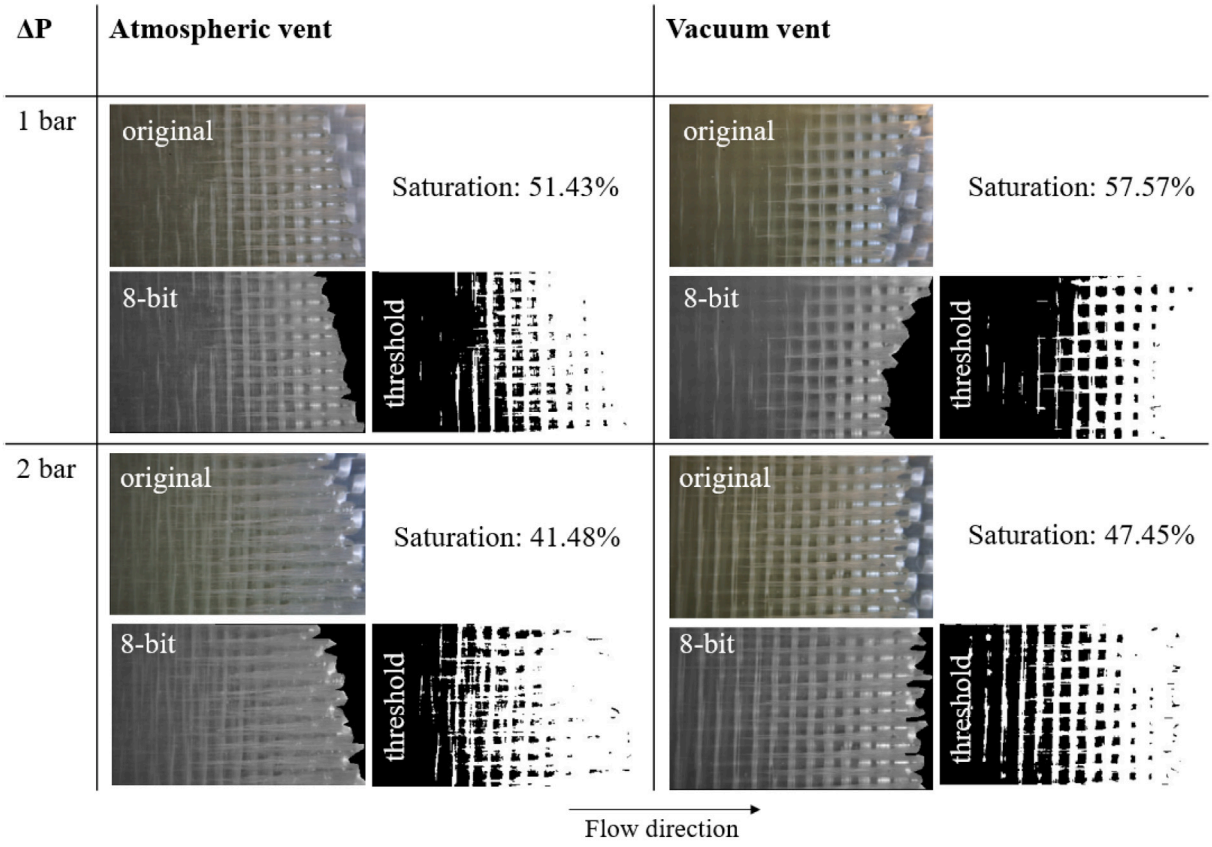

Fig. 11. Comparison of dual scale for QUD 0/90 for atmospheric and vacuum conditions and for pressure difference of 1 and 2 bars. For all the images the portion of dry preform is excluded and the image is converted to 8-bit. After that the threshold is set and portion of saturated preform is obtained.

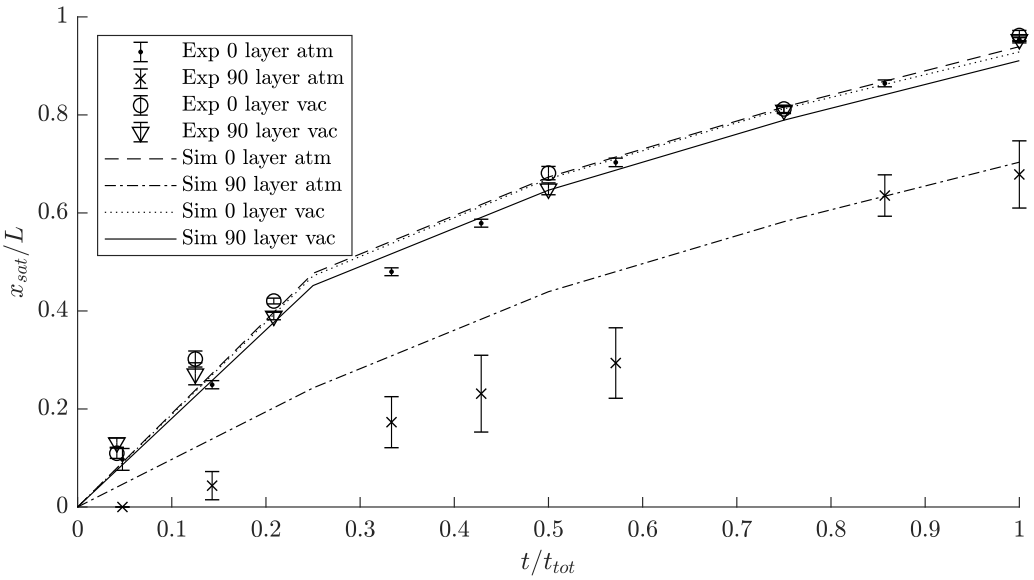

Fig. 12. Results of simulation and experiments for QUD 0/90 for atmospheric and vacuum outlet conditions.

Results of this study are shown in Fig. 15, where the % of unsaturated area represent the evolution of saturation including void entrapment towards the end of the simulation.

Capillary pressure strongly influences filling in the first phases of the process, where flow front pressure is low and thus the resin saturates the preform slowly. This is important particularly for filling of long parts especially for processes requiring a vacuum bag, where the pressure decays over length and speed of filling decreases drastically. The application of correct boundary conditions also has an impact on outcomes of the model, showing how dual scale difference between vacuum and atmospheric outlet also impacts flow behavior at the mesoscopic level. In Fig. 16 the results of filling under atmospheric

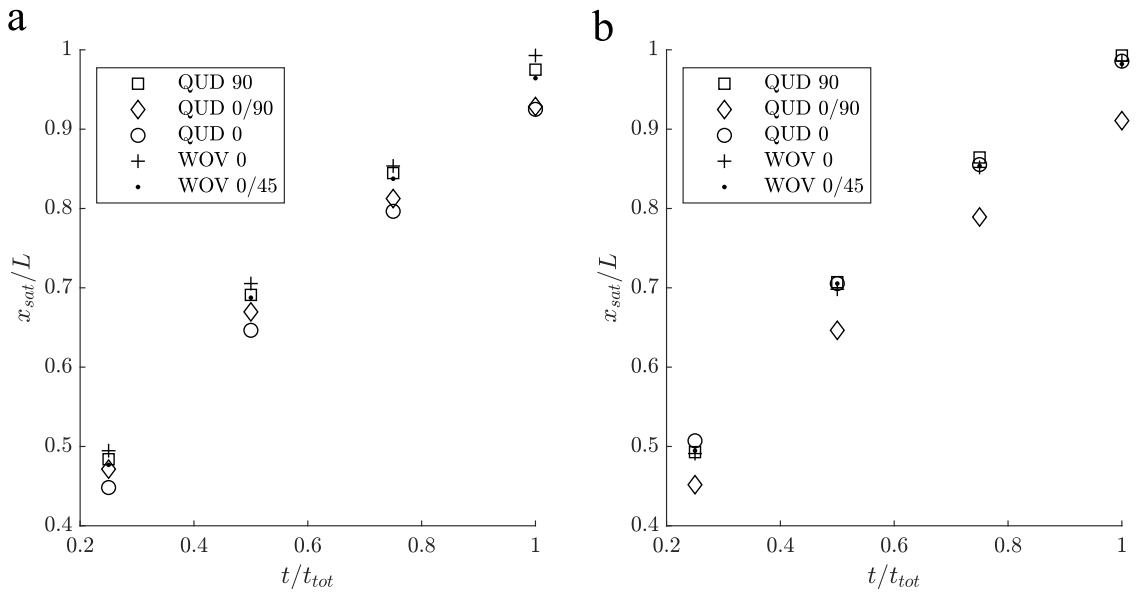

Fig. 13. Simulation results for all the layups for vacuum outlet conditions: layers in 0° (a) and layers in other directions (b).

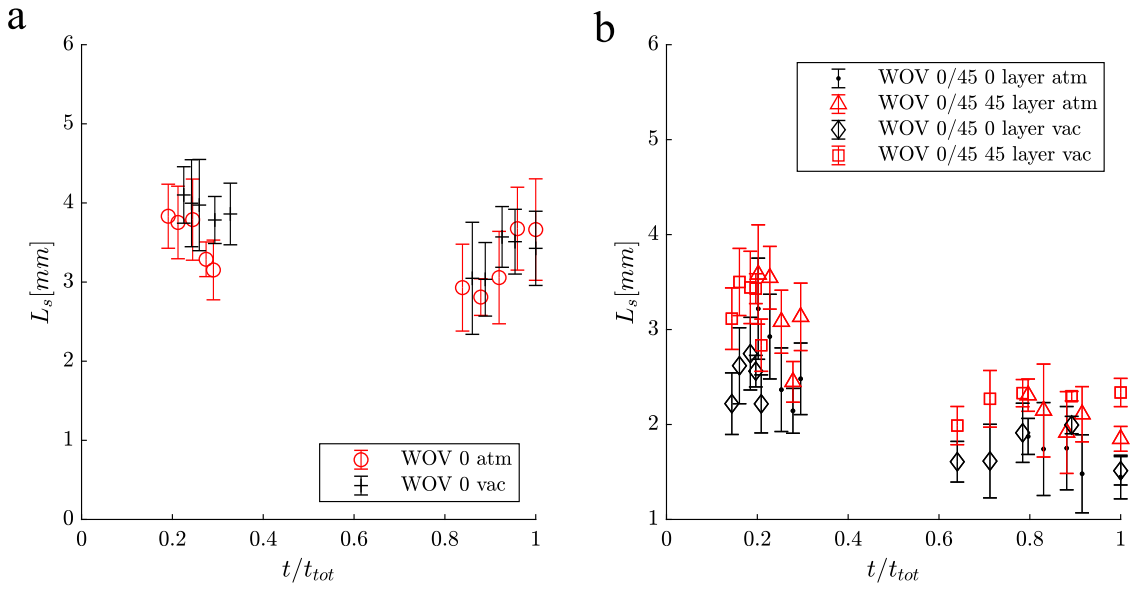

Fig. 14. Comparison of vacuum and atmospheric vent influence on dual scale length Ls for WOV 0 (a) Ca ≈ 0.0024–0.003 and WOV 0/45 (b) Ca ≈ 0.0016–0.0023 (Experiments).

Table 5
Values applied to the simulation for sensitivity study.

ID	$P_{applied}$	P_{cap}	Atmospheric	Vacuum
1 - atm	Linear gradient	0	Yes	–
1 - vac	Linear gradient	0	–	Yes
2 - atm	Linear gradient	5000 Pa only in transverse tows	Yes	–
2 - vac	Linear gradient	5000 Pa only in transverse tows	–	Yes
3 - atm	Linear gradient	5000 Pa only in longitudinal tows	Yes	–
3 - vac	Linear gradient	5000 Pa only in longitudinal tows	–	Yes
4 - atm	Linear gradient	P_{cap} measured in the experiments	Yes	–
4 - vac	Linear gradient	P_{cap} measured in the experiments	–	Yes
5 - atm	Macro model	P_{cap} measured in the experiments	Yes	–
5 - vac	Macro model	P_{cap} measured in the experiments	–	Yes

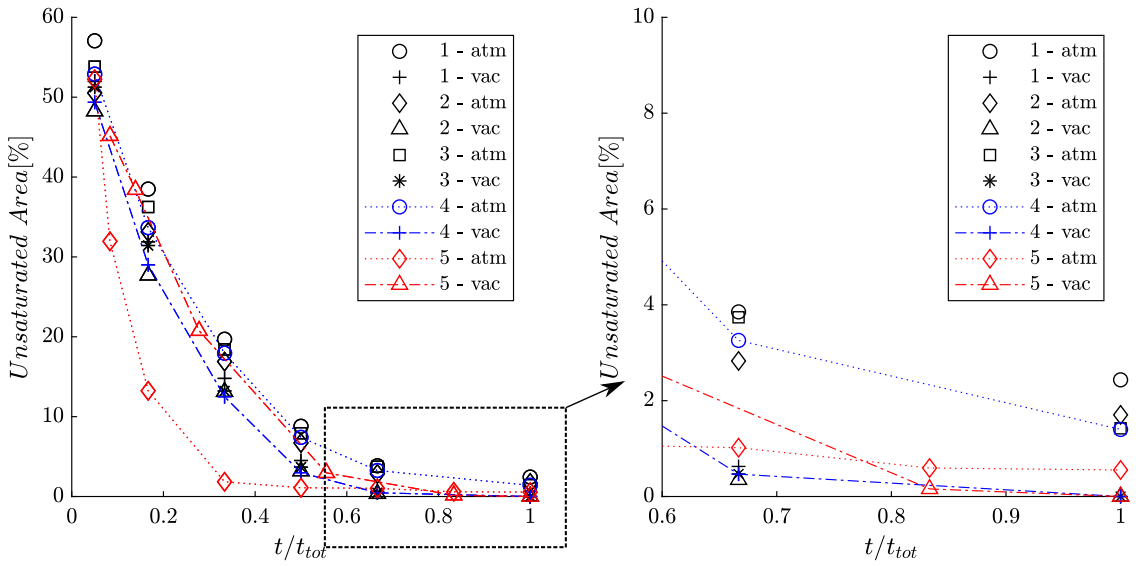

Fig. 15. Sensitivity study for QUD 0/90 layup applying the capillary pressure values mentioned in Table 5 under both vacuum and atmospheric conditions and applying pressure obtained with the macro model (a). (b): detail of final porosity content (Unsaturated Area) shown in (a) for the last 30 s of filling.

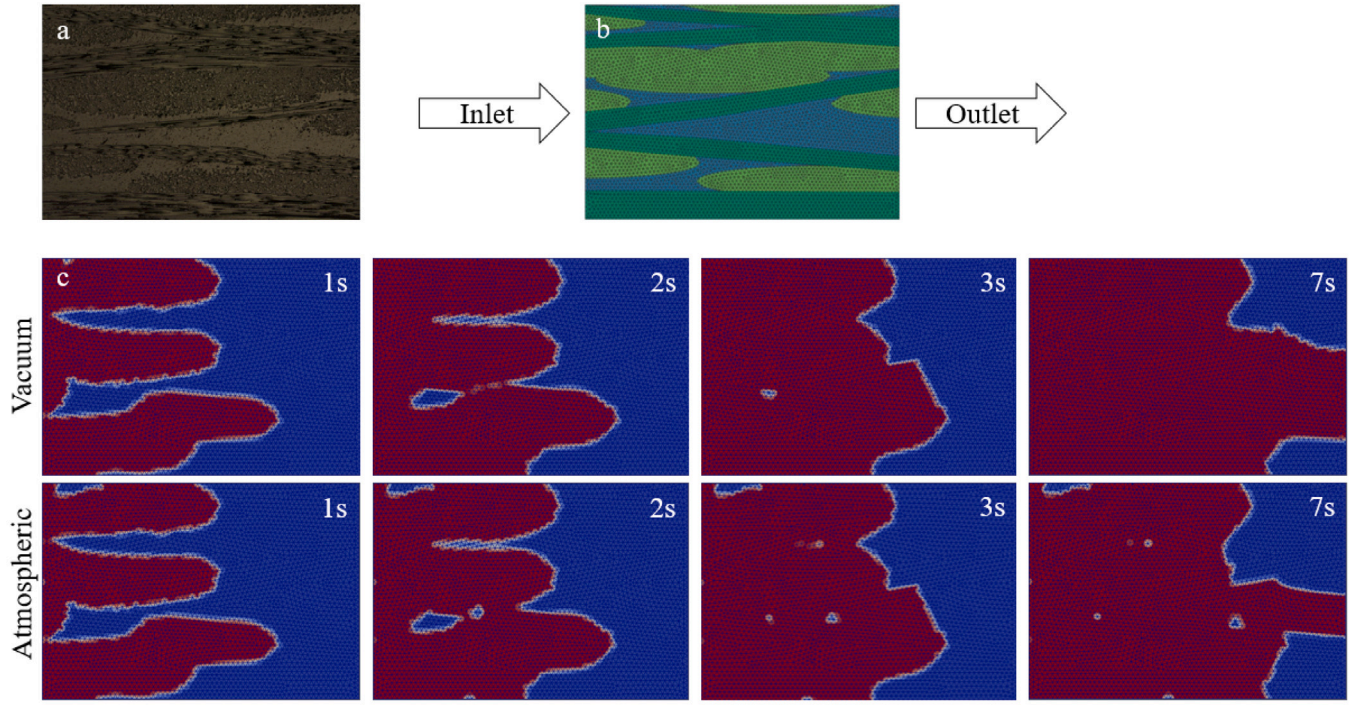

Fig. 16. WOV 0 layup (K_{eff} range: $4.49e^{-9}$ - $4.14e^{-12}$ m^2): (a) microscope picture of the section used to build the model; (b) mesh and boundary conditions location; (c) results comparison between vacuum and atmospheric vent (red: filled elements; blue: empty elements).

and vacuum conditions are compared for the WOV 0 layup. When vent pressure is set to atmospheric, voids are formed in the fiber tows and are later evacuated with the increase of flow pressure (Fig. 16 c, atmospheric).

In Fig. 17 simulation results are compared with time measured for filling a fiber tow at the same position in real tests. Similar trends are found for vacuum conditions. The analysis of further simulation results showed that atmospheric filling required, in general, more time to allow complete evacuation of the pores through void compaction and movement.

A comparison of saturation of tows was performed for all the layups presented in this work and for both atmospheric and vacuum conditions. To compare the simulation models with experimental data, the images obtained during tests were converted to 8-bit images and the area of saturated preform was measured with the help of the open source software Fiji. The selection of a threshold was performed manually to make unsaturated areas visible, as shown in Fig. 18.

This is intended to be a qualitative comparison rather than quantitative, as the planes analyzed are different from experiments (X-Y) to simulations (Y-Z). Results are summarized in Fig. 19. The results

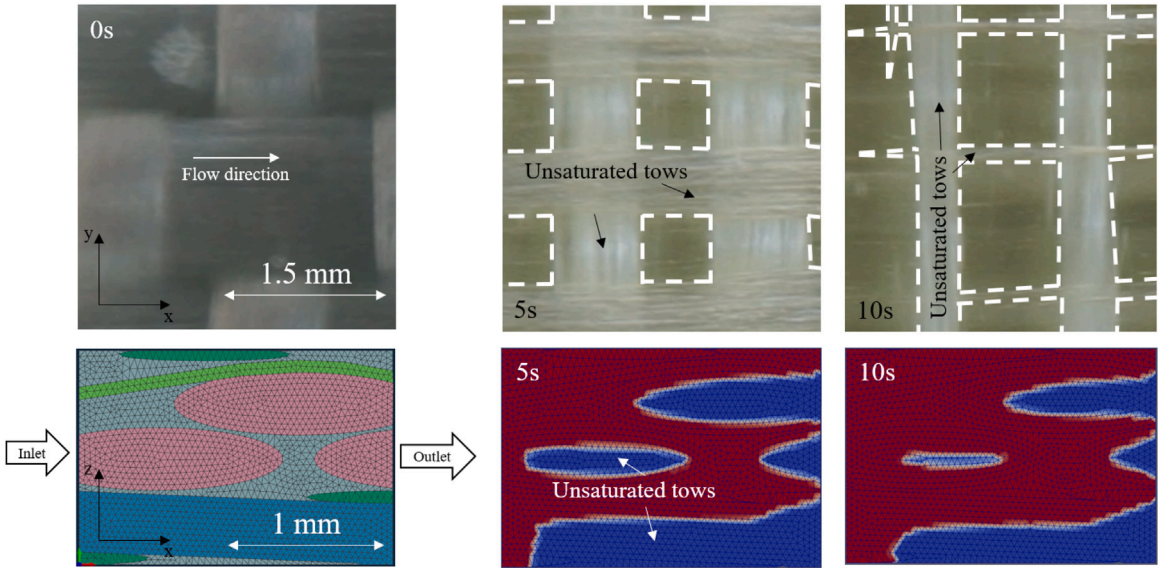

Fig. 17. QUD 0/90 layup, ΔP = 2 bar, vacuum filling: comparison between macro-lens images and simulation model: results at 0, 5 and 10 s of filling of the portion observed.

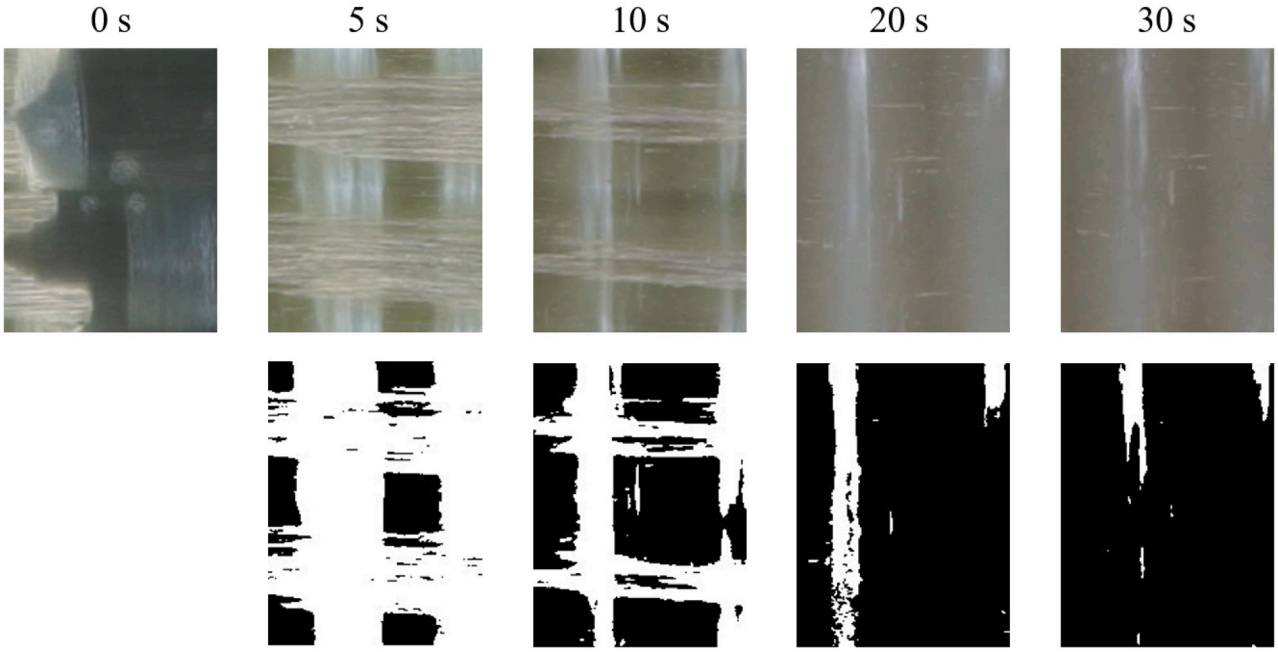

Fig. 18. QUD 0/90 vacuum: Image analysis of the experiments.

obtained with the model depend on accuracy of permeability and thus require further investigation. However, the first estimate for the values calculated seems promising, showing filling time predicted by numerical models to be in a reasonable range. Vacuum simulations results are closer to the experiments, the model in its current state often under predicts voids content for the atmospheric case. Similar trends between experiments and simulation are, however, recognizable. The presence of an atmospheric vent often results in entrapment of voids while, on the other hand, the presence of vacuum leads to complete filling of the mesh. Voids are evacuated only when the flow pressure is sufficient to move them and the presence of air in the tows when filling under atmospheric conditions acts as a block, preventing the saturation of the tows. This effect is not accounted for in the model and could potentially be a topic for further investigation. A possible way to take this effect into account could be to implement a scale factor for permeability to account for the presence of air in the tows.

6. Summary and conclusions

In this work, a method to analyze dual scale flow and void evolution is proposed. The method consists of connecting two FE models in a multiscale approach, so that information gathered in the dual scale simulation (macro) is transferred to the model representing filling of the tows (meso). This is then used to predict saturation and possible void evolution during the process. Both the model representing dual scale and model representing the filling at meso-scale were compared to real tests for two types of reinforcement and for a total of 5 different layups, with the purpose of studying the effect that stacking and preform architecture has on filling results and in particular the dual scale behavior. Layers of fibers sharing the same orientation were grouped in this work to study the effect of tow orientation. However, it has been shown in literature that also stacking order influences dual scale flow [52,53]. This can potentially lead to errors in the simulation and requires further

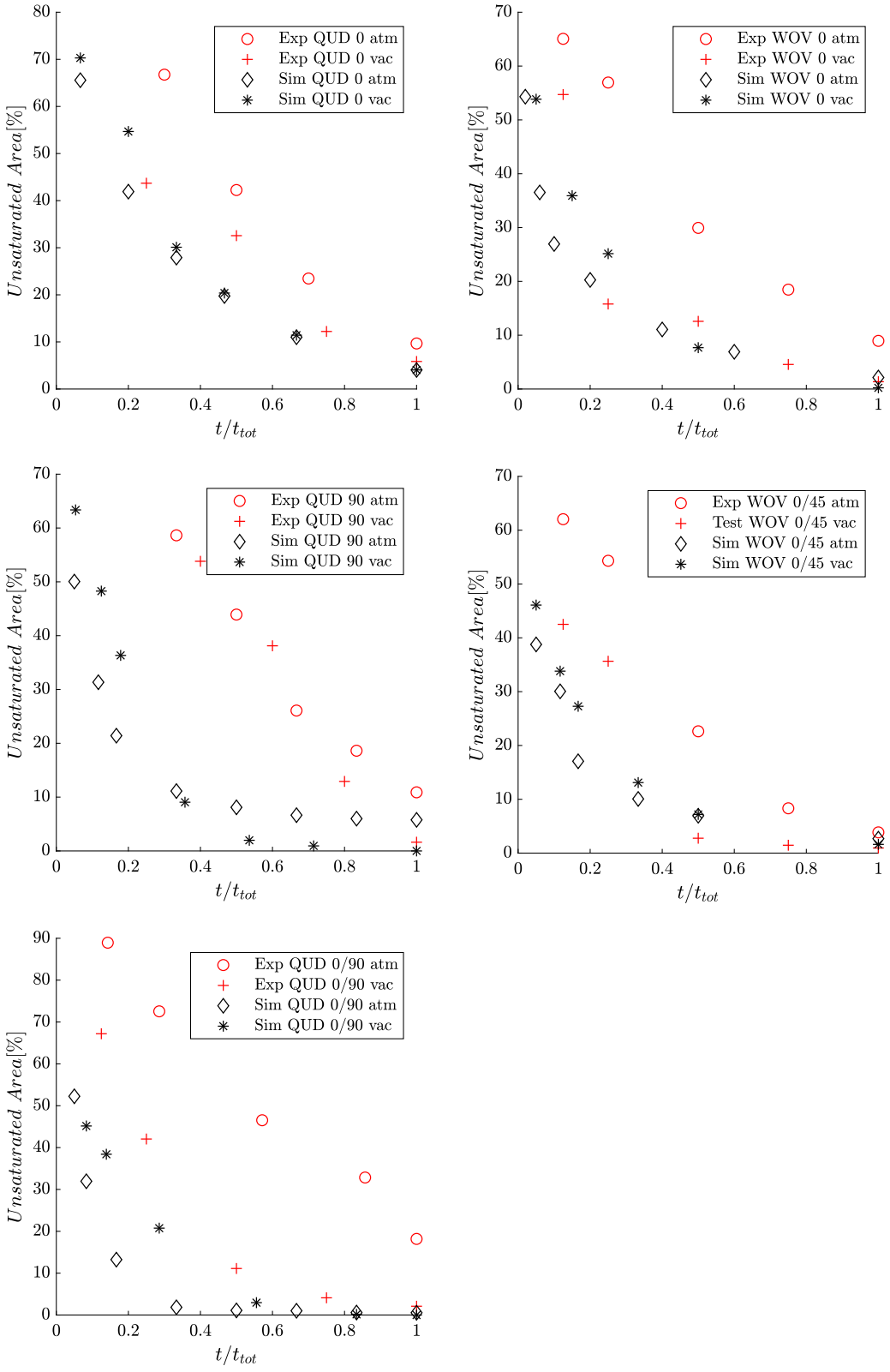

Fig. 19. Mesoscopic model results for all the layups considered under vacuum and atmospheric conditions.

investigation. Nonetheless, the studies performed have confirmed that different materials and layer orientations influence dual scale flow and hence final void content. The analysis of filling under atmospheric and vacuum conditions has also shown that air in the fiber tows leads to formation of voids. These can either move or remain arrested until the part is cured. Although the mesoscopic model often under predicts the amount of voids in the reinforcement for the case of atmospheric vent condition, similar trends to the experimental results are recognizable. This could be attributed to the presence of air inhibiting flow from saturating the tows and requires further investigations. A possible way to take this effect into account could be by means of a scale factor in the permeability values of the tows.

CRediT authorship contribution statement

Silvio Facciotto: Conceptualization, Investigation, Methodology, Software, Validation, Visualization, Writing – original draft, Writing – review & editing. **Pavel Simacek:** Conceptualization, Methodology, Software, Supervision, Writing – review & editing, Resources. **Suresh G. Advani:** Conceptualization, Supervision, Writing – review & editing, Resources, Funding acquisition. **Anthony Pickett:** Supervision, Writing – review & editing, Funding acquisition. **Peter Middendorf:** Supervision, Writing – review & editing, Resources, Funding acquisition.

Declaration of competing interest

The authors declare that they have no known competing financial interests or personal relationships that could have appeared to influence the work reported in this paper.

Data availability

Data will be made available on request.

Acknowledgments

The present work is funded by the Deutsche Forschungsgemeinschaf (DFG, German Research Foundation), Germany - Project number: 432847151 and partially funded by National Science Foundation (USA). NSF Organization: CMMI Div. of Civil, Mechanical, & Manufacturing Innovation Award No.: 2023323 which are gratefully acknowledged by the authors.

References

[1] Mehdikhani M, Gorbatikh L, Verpoest I, Lomov SV. Voids in fiber-reinforced polymer composites: A review on their formation, characteristics, and effects on mechanical performance. J Compos Mater 2019;53(12):1579–669. http://dx.doi.org/10.1177/0021998318772152.

[2] Tang J-M, Lee WI, Springer GS. Effects of cure pressure on resin flow, voids, and mechanical properties. J Compos Mater 1987;21(5):421–40. http://dx.doi.org/10.1177/002199838702100502.

[3] Jeong H. Effects of voids on the mechanical strength and ultrasonic attenuation of laminated composites. J Compos Mater 1997;31(3):276–92. http://dx.doi.org/10.1177/002199839703100303.

[4] Guo Z-S, Liu L, Zhang B-M, Shanyi D. Critical void content for thermoset composite laminates. J Compos Mater 2009;43(17):1775–90. http://dx.doi.org/10.1177/0021998306065289.

[5] Olivier P, Cottu JP, Ferret B. Effects of cure cycle pressure and voids on some mechanical properties of carbon/epoxy laminates. Composites 1995;26(7):509–15. http://dx.doi.org/10.1016/0010-4361(95)96808-J.

[6] Lambert J, Chambers AR, Sinclair I, Spearing SM. 3D damage characterisation and the role of voids in the fatigue of wind turbine blade materials. Compos Sci Technol 2012;72(2):337–43. http://dx.doi.org/10.1016/j.compscitech.2011.11.023.

[7] Carraro PA, Maragoni L, Quaresimin M. Influence of manufacturing induced defects on damage initiation and propagation in carbon/epoxy NCF laminates. Adv Manuf: Polym Compos Sci 2015;1(1):44–53. http://dx.doi.org/10.1179/2055035914Y.0000000004.

[8] Ruiz E, Achim V, Soukane S, Trochu F, Bréard J. Optimization of injection flow rate to minimize micro/macro-voids formation in resin transfer molded composites. Compos Sci Technol 2006;66(3):475–86. http://dx.doi.org/10.1016/j.compscitech.2005.06.013.

[9] Leclerc JS, Ruiz E. Porosity reduction using optimized flow velocity in resin transfer molding. Composites A 2008;39(12):1859–68. http://dx.doi.org/10.1016/j.compositesa.2008.09.008.

[10] Bruschke MV, Advani SG. A numerical approach to model non-isothermal viscous flow through fibrous media with free surfaces. Internat J Numer Methods Fluids 1994;19(7):575–603. http://dx.doi.org/10.1002/fld.1650190704.

[11] Gommer F, Endruweit A, Long AC. Influence of the micro-structure on saturated transverse flow in fibre arrays. J Compos Mater 2018;52(18):2463–75. http://dx.doi.org/10.1177/0021998317747954.

[12] Yazdchi K, Srivastava S, Luding S. Microstructural effects on the permeability of periodic fibrous porous media. Int J Multiph Flow 2011;37(8):956–66. http://dx.doi.org/10.1016/j.ijmultiphaseflow.2011.05.003.

[13] Facciotto S, Simacek P, Advani SG, Middendorf P. Modeling of anisotropic dual scale flow in RTM using the finite elements method. Composites B 2021;214:108735. http://dx.doi.org/10.1016/j.compositesb.2021.108735.

[14] Patel N, Lee LJ. Effects of fiber mat architecture on void formation and removal in liquid composite molding. Polym Compos 1995;16(5):386–99. http://dx.doi.org/10.1002/pc.750160507.

[15] Park CH, Woo L. Modeling void formation and unsaturated flow in liquid composite molding processes: a survey and review. J Reinf Plast Compos 2011;30(11):957–77. http://dx.doi.org/10.1177/0731684411411338.

[16] Lystrup C, George A, Zobell B, Boster K, Childs C, Girod H, et al. Optical measurement of voids in situ during infusion of carbon reinforcements. J Compos Mater 2020;002199832095982. http://dx.doi.org/10.1177/0021998320959820.

[17] Staffan Lundström T, Frishfelds V, Jakovics A. Bubble formation and motion in non-crimp fabrics with perturbed bundle geometry. Composites A 2010;41(1):83–92. http://dx.doi.org/10.1016/j.compositesa.2009.05.012.

[18] Teixidó H, Staal J, Caglar B, Michaud V. Capillary effects in fiber reinforced polymer composite processing: A review. Front Mater 2022;44. http://dx.doi.org/10.3389/fmats.2022.809226.

[19] Michaud V. A review of non-saturated resin flow in liquid composite moulding processes. Transp Porous Media 2016;115(3):581–601. http://dx.doi.org/10.1007/s11242-016-0629-7.

[20] Ahn KJ, Seferis JC, Berg JC. Simultaneous measurements of permeability and capillary pressure of thermosetting matrices in woven fabric reinforcements. Polym Compos 1991;12(3):146–52. http://dx.doi.org/10.1002/pc.750120303.

[21] Pillai KM, Advani SG. Wicking across a Fiber-Bank. J Colloid Interface Sci 1996;183(1):100–10. http://dx.doi.org/10.1006/jcis.1996.0522.

[22] Amico SC, Lekakou C. Axial impregnation of a fiber bundle. Part 1: Capillary experiments. Polym Compos 2002;23(2):249–63. http://dx.doi.org/10.1002/pc.10429.

[23] Matsuzaki R, Seto D, Naito M, Todoroki A, Mizutani Y. Analytical prediction of void formation in geometrically anisotropic woven fabrics during resin transfer molding. Compos Sci Technol 2015;107:154–61. http://dx.doi.org/10.1016/j.compscitech.2014.12.013.

[24] Vilà J, Sket F, Wilde F, Requena G, González C, LLorca J. An in situ investigation of microscopic infusion and void transport during vacuum-assisted infiltration by means of X-ray computed tomography. Compos Sci Technol 2015;119:12–9. http://dx.doi.org/10.1016/j.compscitech.2015.09.016.

[25] Willenbacher B, May D, Mitschang P. Out–of–plane capillary pressure of technical textiles. Composites A 2019;124:105495. http://dx.doi.org/10.1016/j.compositesa.2019.105495.

[26] Bayramli E, Powell R. The normal (transverse) impregnation of liquids into axially oriented fiber bundles. J Colloid Interface Sci 1990;138(2):346–53. http://dx.doi.org/10.1016/0021-9797(90)90217-C.

[27] Yeager M, Hwang WR, Advani SG. Prediction of capillary pressure for resin flow between fibers. Compos Sci Technol 2016;126:130–8. http://dx.doi.org/10.1016/j.compscitech.2016.02.014.

[28] Yeager M, Simacek P, Advani SG. Role of fiber distribution and air evacuation time on capillary driven flow into fiber tows. Composites A 2017;93:144–52. http://dx.doi.org/10.1016/j.compositesa.2016.11.016.

[29] Li C, Cantarel A, Gong X. A study on resin infusion and effects of reinforcement structure at dual scales by a quasi-realistic numerical simulation method. J Compos Mater 2020;54(27):4157–71. http://dx.doi.org/10.1177/0021998320926707.

[30] Patel N, Lee LJ. Modeling of void formation and removal in liquid composite molding. Part I: Wettability analysis. Polym Compos 1996;17(1):96–103. http://dx.doi.org/10.1002/pc.10594.

[31] Patel N, Lee LJ. Modeling of void formation and removal in liquid composite molding. Part II: Model development and implementation. Polym Compos 1996;17(1):104–14. http://dx.doi.org/10.1002/pc.10595.

[32] Labat L, Bréard J, Pillut-Lesavre S, Bouquet G. Void fraction prevision in LCM parts. Eur Phys J Appl Phys 2001;16(2):157–64. http://dx.doi.org/10.1051/epjap:2001104.

[33] Bréard J, Henzel Y, Trochu F, Gauvin R. Analysis of dynamic flows through porous media. Part I: Comparison between saturated and unsaturated flows in fibrous reinforcements. Polym Compos 2003;24(3):391–408. http://dx.doi.org/10.1002/pc.10038.
[34] Gourichon B, Binetruy C, Krawczak P. A new numerical procedure to predict dynamic void content in liquid composite molding. Composites A 2006;37(11):1961–9. http://dx.doi.org/10.1016/j.compositesa.2005.12.017.
[35] Simacek P, Advani SG. A numerical model to predict fiber tow saturation during liquid composite molding. Compos Sci Technol 2003;63(12):1725–36. http://dx.doi.org/10.1016/S0266-3538(03)00155-6.
[36] Bayldon JM, Daniel IM. Flow modeling of the VARTM process including progressive saturation effects. Composites A 2009;40(8):1044–52. http://dx.doi.org/10.1016/j.compositesa.2009.04.008.
[37] Lawrence JM, Neacsu V, Advani SG. Modeling the impact of capillary pressure and air entrapment on fiber tow saturation during resin infusion in LCM. Composites A 2009;40(8):1053–64. http://dx.doi.org/10.1016/j.compositesa.2009.04.013.
[38] Simacek P, Neacsu V, Advani SG. A phenomenological model for fiber tow saturation of dual scale fabrics in liquid composite molding. Polym Compos 2010;31(11):1881–9. http://dx.doi.org/10.1002/pc.20982.
[39] Park CH, Lebel A, Saouab A, Bréard J, Lee WI. Modeling and simulation of voids and saturation in liquid composite molding processes. Composites A 2011;42(6):658–68. http://dx.doi.org/10.1016/j.compositesa.2011.02.005.
[40] Tan H, Pillai KM. Multiscale modeling of unsaturated flow in dual-scale fiber preforms of liquid composite molding III: reactive flows. Composites A 2012;43(1):29–44. http://dx.doi.org/10.1016/j.compositesa.2011.08.008.
[41] Carlone P, Rubino F, Paradiso V, Tucci F. Multi-scale modeling and online monitoring of resin flow through dual-scale textiles in liquid composite molding processes. Int J Adv Manuf Technol 2018;96(5–8):2215–30. http://dx.doi.org/10.1007/s00170-018-1703-9.
[42] Wu D, Larsson R. A shell model for resin flow and preform deformation in thin-walled composite manufacturing processes. Int J Mater Form 2020;13(6):923–37. http://dx.doi.org/10.1007/s12289-019-01517-z.
[43] Patiño Arcila I, Power H, Nieto Londoño C, Flórez Escobar W. Boundary element method for the dynamic evolution of intra-tow voids in dual-scale fibrous reinforcements using a Stokes–Darcy formulation. Eng Anal Bound Elem 2018;87:133–52. http://dx.doi.org/10.1016/j.enganabound.2017.11.014.
[44] Pillai KM, Advani SG. Numerical simulation of unsaturated flow in woven fiber preforms during the resin transfer molding process. Polym Compos 1998;19(1):71–80. http://dx.doi.org/10.1002/pc.10077.
[45] DeValve C, Pitchumani R. Simulation of void formation in liquid composite molding processes. Composites A 2013;51:22–32. http://dx.doi.org/10.1016/j.compositesa.2013.03.016.
[46] Gascón L, García JA, LeBel F, Ruiz E, Trochu F. Numerical prediction of saturation in dual scale fibrous reinforcements during liquid composite molding. Composites A 2015;77:275–84. http://dx.doi.org/10.1016/j.compositesa.2015.05.019.
[47] Liu Y, Moulin N, Bruchon J, Liotier P-J, Drapier S. Towards void formation and permeability predictions in LCM processes: A computational bifluid–solid mechanics framework dealing with capillarity and wetting issues. C R Mécanique 2016;344(4–5):236–50. http://dx.doi.org/10.1016/j.crme.2016.02.004.
[48] Kang MK, Lee WI, Hahn HT. Formation of microvoids during resin-transfer molding process. Compos Sci Technol 2000;60(12):2427–34. http://dx.doi.org/10.1016/S0266-3538(00)00036-1.
[49] Aaboud B, Saouab A, Nawab Y. Simulation of air bubble's creation, compression, and transport phenomena in resin transfer moulding. J Compos Mater 2017;51(29):4115–27. http://dx.doi.org/10.1177/0021998317697481.
[50] Aaboud B, Bizet L, Saouab A, Nawab Y. Effect of the spatial variation of permeability on air bubble creation and compression. J Reinf Plast Compos 2020;39(7–8):285–98. http://dx.doi.org/10.1177/0731684419899475.
[51] Kuentzer N, Simacek P, Advani SG, Walsh S. Permeability characterization of dual scale fibrous porous media. Composites A 2006;37(11):2057–68. http://dx.doi.org/10.1016/j.compositesa.2005.12.005.
[52] Adams KL, Rebenfeld L. Permeability characteristics of multilayer fiber reinforcements. Part I: Experimental observations. Polym Compos 1991;12(3):179–85. http://dx.doi.org/10.1002/pc.750120307.
[53] Bancora SP, Binetruy C, Advani SG, Syerko E, Comas-Cardona S. Effective permeability averaging scheme to address in-plane anisotropy effects in multi-layered preforms. Composites A 2018;113:359–69. http://dx.doi.org/10.1016/j.compositesa.2018.07.025.
[54] Zhou F, Kuentzer N, Simacek P, Advani SG, Walsh S. Analytic characterization of the permeability of dual-scale fibrous porous media. Compos Sci Technol 2006;66(15):2795–803. http://dx.doi.org/10.1016/j.compscitech.2006.02.025.
[55] Gebart BR. Permeability of unidirectional reinforcements for RTM. J Compos Mater 1992;26(8):1100–33. http://dx.doi.org/10.1177/002199839202600802.
[56] Godbole MG, Gururaja S, Joshi M, Advani S. Semi-analytical formulation of effective permeability of a dual scale unidirectional fabric. Composites A 2021;150:106630. http://dx.doi.org/10.1016/j.compositesa.2021.106630.
[57] Dittmann J. Numerische Multiskalen-Permeabilitätsvorhersage von endkonturnahen textilen Fasermodellen. 2022.
[58] Caglar B, Tekin C, Karasu F, Michaud V. Assessment of capillary phenomena in liquid composite molding. Composites A 2019;120:73–83. http://dx.doi.org/10.1016/j.compositesa.2019.02.018.
[59] Amico S, Lekakou C. Mathematical modelling of capillary micro-flow through woven fabrics. Composites A 2000;31(12):1331–44. http://dx.doi.org/10.1016/S1359-835X(00)00033-6.
[60] Mhetre S, Parachuru R. The effect of fabric structure and yarn-to-yarn liquid migration on liquid transport in fabrics. J Text Inst 2010;101(7):621–6. http://dx.doi.org/10.1080/00405000802696469.
[61] Monaenkova D, Andrukh T, Kornev KG. Bernoulli catenary and elasto-capillary effect in partially wet fibrous materials. Text Res J 2013;83(13):1386–97. http://dx.doi.org/10.1177/0040517512464294.
[62] Pucci MF, Liotier P-J, Drapier S. Capillary wicking in a fibrous reinforcement – orthotropic issues to determine the capillary pressure components. Composites A 2015;77:133–41. http://dx.doi.org/10.1016/j.compositesa.2015.05.031.
[63] LeBel F, Fanaei AE, Ruiz É, Trochu F. Prediction of optimal flow front velocity to minimize void formation in dual scale fibrous reinforcements. Int J Mater Form 2014;7(1):93–116. http://dx.doi.org/10.1007/s12289-012-1111-x.